



Highly turbulent counterflow flames: A laboratory scale benchmark for practical systems

Gianfilippo Coppola¹, Bruno Coriton, Alessandro Gomez*

Department of Mechanical Engineering, Yale Center for Combustion Studies, Yale University, P.O. Box 208286, New Haven, CT 06520-8286, USA

ARTICLE INFO

Article history:

Received 8 January 2009

Received in revised form 12 February 2009

Accepted 25 March 2009

Available online 7 July 2009

Keywords:

Counterflow

Opposed jet

Turbulent flames

ABSTRACT

We propose a highly *turbulent counterflow flame* as a very useful benchmark of complexity intermediate between laminar flames and practical systems. By operating in a turbulent Reynolds number regime of relevance to practical systems such as gas turbines and internal combustion engines, it retains the interaction of turbulence and chemistry of such environments, but offers several advantages including: (a) the achievement of high Reynolds numbers without pilot flames, which is particularly advantageous from a modeling standpoint; (b) control of the transition from stable flames to local extinction/reignition conditions; (c) compactness of the domain by comparison with jet flames, with obvious advantages from both a diagnostic and, especially, a computational viewpoint; and (d) the reduction or, altogether, elimination of soot formation, thanks to the high strain rates and low residence times of such a system, and the establishment of conditions of large stoichiometric mixture fraction, as required for robust flame stabilization. We demonstrate the phenomenology of such highly strained turbulent flames under conditions spanning unpremixed, partially premixed and premixed regimes. The system lends itself to the validation of DNS and other computational models. It is also well-suited for the examination of practical fuel blends – a need that is becoming more and more pressing in view of the anticipated diversification of the future fossil fuel supply.

© 2009 The Combustion Institute. Published by Elsevier Inc. All rights reserved.

1. Introduction

The counterflow system has been extensively studied for the past three decades under laminar conditions both under steady and unsteady conditions, but, it is a relatively recent addition to the field of turbulent combustion through the effort of a few groups, mostly outside the U.S. It has *not* been one of the benchmark flames in the turbulent combustion workshops [1,2]. Without attempting to do justice to the huge body of literature on turbulent combustion, for which the reader can examine a number of reviews [3–7], the most relevant work on freestanding flames in stagnating turbulence spanned the past four decades [8–27]. It covered both premixed [8,13–16,24,25,27] and non-premixed [9–12,17–22,26] flames, including both experimental and modeling contributions, with the work from the group in Darmstadt being the most comprehensive investigation to date [19–22]. The drawback of all these studies is that their turbulent Reynolds numbers tend to be low, being typically below 100. Consequently, the turbulence is weak, which makes these experiments of modest relevance to practical applications. Possibly, this is the reason why such a system was not embraced by the combustion community.

If the flames are sufficiently strained, local extinction can manifest itself with the appearance of non-reactive holes. The phenomenon was observed first in [15] for premixed flames and linked to the total stretch rate experienced by the flame, accounting for both the mean and fluctuating component. Similar phenomena were reported in non-premixed flames and also linked to the total strain rate experienced by the flame [20]. In these flames the scalar dissipation rate at extinction provides the critical (inverse) time for extinction. From the flamelet perspective of turbulent combustion, the time history of the strain rate determines the effective scalar dissipation rate felt by the flame. As soon as the flame locally extinguishes and a non-reactive hole appears, a partially premixed edge flame forms in an area of relatively high velocity and turbulence. Alternatively, possibly autoignition may play a role in the reignition of locally extinguished regions, depending on the local temperature of the mixture. A systematic study of these extinction/ignition phenomena is of direct relevance to flame stabilization and is well suited to the counterflow configuration.

We present here a bench-top flame configuration of the *turbulent counterflow flame* (TCF) that overcomes some of the limitations of previous work. By improving the design of the turbulence generation system and selecting judiciously the feed stream composition, we achieved high Reynolds numbers, comparable to those of engines and gas turbines. The advantages that this configuration has to offer with respect to the extensively tested free-jet counterpart

* Corresponding author. Fax: +1 203 432 7654.

E-mail address: alessandro.gomez@yale.edu (A. Gomez).

¹ Present address: Department of Bioengineering, Imperial College, London, UK.

are discussed. After showing evidence of the healthy turbulence that the system can achieve, we demonstrate the richness of phenomenology that we observed in a broad range of regimes from non-premixed to premixed flames. In view of the compactness of this configuration, the TCF is proposed as a benchmark for testing and validating computational models, including direct numerical simulation, as demonstrated by a comparison of the size of the domain with the all too common co-flow (jet) flame at comparable turbulent Reynolds number (Re_t). We conclude by arguing that this configuration is uniquely suited for the study of turbulent combustion of more challenging fuels, as compared to the ubiquitous methane and hydrogen that have characterized the bulk of turbulent combustion research to date.

2. TCF PROS and CONS

Advantages of a stagnating turbulent flow, in part reviewed in [23], are:

- Simplicity and versatility of the experimental setup, allowing for the exploration of a range of important scenarios, from near-equilibrium to extinction conditions, in a broad range of Damköhler numbers.
- Elimination of the influence of nearby surfaces and/or pilot flames to anchor the flame, since flame stabilization is achieved aerodynamically in the vicinity of the stagnation plane.
- Compactness, with characteristic dimensions of the flow field on the order of some centimeters, as opposed to turbulent jet flames with dimensions typically 1 or 2 orders of magnitude larger. This feature is convenient both diagnostically and computationally.
- Suitability for the study the combustion of fuels more “challenging” from a chemical kinetic viewpoint than hydrogen or methane, which have absorbed much of the turbulent combustion community so far, in part to avoid soot complications.

To elaborate on the points above, we note that the configuration can be varied easily from a fully non-premixed to a partially premixed and ultimately fully premixed system. As a result, separate testing of models are possible for all these systems, with the same inflow conditions but different composition of the feed streams. The small system length scale is convenient from a diagnostic viewpoint, since imaging of virtually the entire combustion region can be collected by planar laser diagnostic techniques. From a computational perspective, the flame compactness allows for simulations using a relatively small computational mesh. As a result, highly resolved simulations might become affordable, grid- and, in the case of LES, filter-dependence of the models can be studied systematically. The high strain rates at which the counterflow flames can be operated (see below) result in overall residence times shorter than those necessary for soot to form. Soot would otherwise be unavoidable in conventional jet flames of heavier hydrocarbons, at least under non-premixed conditions, except if highly diluted flames could be stabilized, which is usually a challenge. We also note that the counterflow system can be analyzed theoretically through a relatively manageable system of ordinary differential equations, as shown, for example in [24], which could add another dimension to the understanding of these flow fields, beyond the computational approach. Conventional experimental configurations, such as turbulent jets, are much more limited with respect to all of these opportunities.

As evidenced by the existing literature, there are criticisms, which might explain some reluctance of the community to embrace this configuration. It is often argued that the configuration is artificial and seemingly removed from practical combustion

problems. In this respect, we note that decelerating and/or highly strained velocity fields are present in many practical situations. The counterflow configuration is actually used for the stabilization of flames in aerocombustor cans. Also, stagnation flows do occur under vortex break down conditions that are typical of the stabilization mechanism of modern swirl-stabilized lean premixed and non-premixed spray combustion systems [28]. In the initial region of turbulent jets, a strongly strained mixing layer is present in the “braid” region and, to a moving observer, counterflow conditions appear between counter-rotating streamwise vortices. As a result, to study systematically the combustion behavior in stagnating turbulence is practically relevant. Additional criticisms, e.g., modest turbulence level and young [26,27] turbulence, are best refuted when we present some results under cold conditions.

3. Experimental setup

3.1. Flow system

Under non-premixed conditions the counterflow burner is realized by placing two exact copies of the same coflowing jet nozzles one inner nozzle diameter away from each other (Fig. 1a). Each jet assembly consists of a 12.6 mm diameter inner nozzle (d_i) and a 26.9 mm inner diameter outer nozzle (d_o). The nozzles are $0.75d_i$ apart from each other. A large variety of turbulence generation systems was investigated and a plate (Fig. 1b) with a 0.9 blockage was chosen for the present investigation. The plate is characterized by a convoluted central opening, resembling the exit section of lobed nozzles, which generates a set of jets near the axis of the nozzle. Further details on the relative performance of a variety of plates and their induced turbulent flow field are given in a companion paper under review. Different from [9–22], the plate is positioned *upstream* of the contraction terminating with the burner outlet, consistently with the design of [29]. The nozzle is characterized by a smoothly contoured profile, which produces uniform flow

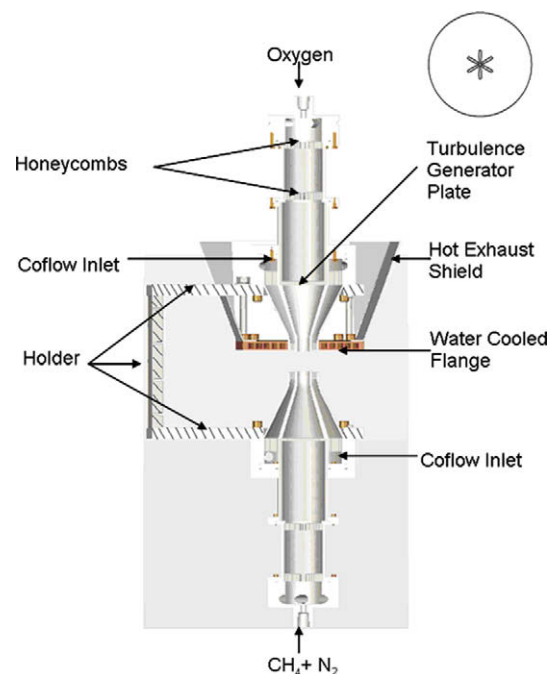


Fig. 1. Burner configuration for non-premixed flames. The same burner can be operated in the premixed mode by feeding premixed mixtures of identical composition from both top and bottom halves. Also shown on the side is the geometry of the turbulence generation plate.

conditions at the exit section. Boundary layer separation was not an issue in the presence of the turbulence generator, because of the central position of the jet issuing from the plate. An annular co-flow of nitrogen with a mass averaged velocity of about 6.4 m/s, is used on both sides to quench partially the flame. The contoured design of the co-flow nozzle, coupled to 1/64th cell size honeycombs, guarantees an exit velocity profile with reasonable uniformity. Under the present conditions (stoichiometric mixture fraction $Z_f = 0.515$, 35% CH_4 in N_2 in the fuel stream and 100% O_2 in the oxidizer stream) the mass averaged velocities reaches 13 m/s with equal momentum in the two streams, resulting in engineering Reynolds numbers, $Re = U d_i/\nu$, of up to 10^4 , based on the inner nozzle diameter (d_i), and a bulk strain rate, $a \sim 2.5 \times 10^3 \text{ s}^{-1}$. The flow rate is controlled by digital flow controllers (Teledyne-Hastings 300D series) providing a readout accuracy of $\pm 0.5\%$ and a full scale one of $+0.2\%$. Various experimental conditions are investigated for the same feed stream composition, ranging from the absence of turbulence generator from either one or both nozzles, to the condition of most intense turbulence, with identical generators in both streams. Experiments are conducted under both cold flow and burning conditions.

The same burner can be used also under premixed and partially premixed conditions. In such a case two identical premixed streams are fed to top and bottom burner and twin flames are established symmetrically with respect to the gas stagnation plane, in the turbulent analogue of a configuration that has been extensively studied under laminar conditions [30].

3.2. Measurement techniques and data analysis

3.2.1. Hot wire anemometry

Turbulence characteristics are derived from velocity measurements by hot-wire anemometry, with the probe positioned at the nozzle centerline, 0.5 mm above the bottom nozzle exit section. A high frequency (up to 150 kHz) response anemometer (IFA 100, TSI Inc.) is used with a single sensor probe (TSI, Inc. Model 1212) made of a 5 μm diameter (d_w) silver coated platinum wire with a 1.27 mm sensitive length (l_w), resulting in an $l_w/d_w \sim 250$. The hot wire is calibrated using a unit (TSI, Inc. Model 1125) consisting of a contoured nozzle, producing a very flat and laminar flow at the exit section, a pressure transducer, allowing for a very accurate measurement of the flow rate, and a probe holder, to position the sensitive wire at the center of the nozzle exit section and perpendicular to the flow. All the data are sampled at the maximum sampling frequency allowed by the data acquisition board $f_s = 200 \text{ kHz}$ and high-pass filtered at $f_a = f_s/2 = 100 \text{ kHz}$ to prevent aliasing. The length of each record is chosen to be the largest allowed by the system memory capability, which resulted in records of up to 8.4×10^6 points ($\sim 65,000$ integral time scales). The one-dimensional power spectrum in the frequency space, $E_1(f)$, is estimated by the Welch method [31], by which, after dividing the record in many sub-records (typically ~ 1000) with 50% overlap, the power spectrum is estimated on each sub-record by applying a Hamming window, and averaged over all sub-records. The integral length scale, L , is estimated by fitting the estimated power spectrum with the von Karman's turbulent spectrum [32],

$$\frac{UE_1(f)}{Lu^2} = 4 \left[1 + \left(\frac{8\pi f L}{3U} \right)^2 \right]^{-5/6}, \quad (1)$$

where f is the frequency, u^2 is the velocity variance and U is the mean velocity. The transverse Taylor length scale, λ , is estimated from the mean energy dissipation rate, $\bar{\epsilon}$, according to the equation

$$\lambda = \left(\frac{15\nu u^2}{\bar{\epsilon}} \right)^{1/2}, \quad (2)$$

where ν is the kinematic viscosity [33]. The mean energy dissipation rate, $\bar{\epsilon}$, is estimated by fitting the power spectrum inertial sub-range to the equation [31]

$$E_1\{k_1\} = \frac{18}{55} A \bar{\epsilon}^{2/3} k_1^{-5/3}, \quad (3)$$

where $k_1 = 2\pi f/U$ is the wavenumber and $A = 1.62$ is a constant [32]. The statistical uncertainty is estimated by assuming a general distribution for the samples [33] and 95% confidence. The error propagation rules are applied to estimate the uncertainties in the derived quantities. Conservatively, we assume a $\pm 3\%$ uncertainty related to the apparatus, including calibrator for a single velocity component sample [34]. The errors resulting from high turbulence intensity are also taken into account and estimated from [35]. The resulting total uncertainty comprises the flow metering system uncertainty, the measurement system uncertainty for a single sample, the statistical uncertainty and the uncertainty arising from the turbulence levels effect on the hot wire.

3.2.2. Particle image velocimetry (PIV) and flame front tracking

The two-dimensional flow field is characterized by PIV under cold and burning conditions. Under burning conditions, the flow is seeded by either particles to determine the velocity field or droplets, to infer temperature iso-contours bracketing the flame. In the first case, the flow is seeded by 0.3 μm aluminum oxide particles using a homemade fluidized bed with a cyclone separator, providing a constant supply of particles. In the second case, the flow is seeded by olive oil droplets, generated by a droplet generator placed upstream the nozzle inlet, producing droplets with a narrow size distribution centered at 1.5 μm in diameter. The oil droplets evaporate at 570 K, leaving a dark region in the PIV images, indicating the presence of the flame. In the present experiments, the PIV data are used only qualitatively to infer the location of the high temperature zone and the occurrence of local extinction based on the disappearance/presence of the olive droplets.

As regards to the optical system (manufactured by TSI Inc.), the light beam generated by the laser is made into a laser sheet, through a 500 mm focal length plano-convex lens followed by a 250 mm focal length plano-concave cylindrical lens. The resulting laser sheet, measuring approximately 20 mm in height and $\sim 0.6 \text{ mm}$ in thickness, illuminates the droplets/particles seeded through the nozzles by going through the region of interest. The light scattered by the droplets is then collected by the CCD detector. The PIV system is operated in the cross-correlation mode, thereby requiring two images taken at a very short time separation and a light source able to fire twice at the same short time separation. The camera used is a 12 bit, 2kx2k, cooled CCD (Cook Corp., PCO-20004 Gb) with 4 Gb of on-board memory in double exposure mode, 14.7 Hz max repetition rate in single exposure mode and pixel size of $\sim 7.4 \mu\text{m}$. The PIV image pairs are analyzed using the multi-pass FFT cross-correlation deformation grid algorithm option available in Insight 3 G (TSI Inc.), with vector filtering and smoothing between passes, to maximize resolution and minimize vector dropout. The reader is referred to the Insight 3 G manual for details of the algorithm. The magnification is about 1:1, which results in a field of view of about 15 mm \times 15 mm. The final window size is 32 \times 32 pixels in the cold flow case and 64 \times 64 pixels in the reactive case, respectively equivalent to a physical size of 0.24 \times 0.24 mm and 0.48 \times 0.48 mm which, with 50% overlap, produces a vector every 0.12 mm and 0.24 mm, respectively. All the quantities of interest are derived by analyzing large sets of double exposure images ranging from 308 to 745 in number, which produces a well converged mean and acceptable fluctuating components. With the present size of the interrogation area ($\sim 0.24 \text{ mm}$ and $\sim 0.48 \text{ mm}$) and an estimated integral scale of $\sim 4 \text{ mm}$, the resolution, defined as the ratio between the window size and the inte-

gral scale, is about 0.12 and 0.06, which results in uncertainties in turbulence intensities of less than 10% [36]. A cylindrical coordinate system (r, z) is defined with origin at the mean stagnation point, where $z > 0$ indicate points above the stagnation plane, and $r > 0$ indicate points to the right of the centerline.

3.2.3. Planar laser induced fluorescence (PLIF)

Flame front location and topology in selected experiments are observed by OH Planar Laser Induced Fluorescence (PLIF). To that end, a 3.5 mJ UV laser beam from a Nd:Yag pumped dye laser is tuned to excite the $Q_1(8)$ transition of the (1,0) band of the $A^2\Sigma^+ \leftarrow X^2\Pi$ system at a wavelength of 283.5 nm. The beam is expanded and shaped into a laser sheet by a 300 mm cylindrical quartz lens. The fluorescence signal at 310 nm is imaged on a 1280×1024 ICCD camera (Cooke Dicam-Pro series) through a UV-Nikkor 105 mm f/4.5 UV lens.

4. Results and discussion

4.1. Cold flow testing

Typical radial profiles of the mean axial velocity, as measured by PIV, are shown in Fig. 2 (left) as a function of the distance, z , from the mean position of the stagnation plane. At $z = -7$ mm from the stagnation plane the profile shows the typical M-shape of stagnation point flows. As the flow approaches the stagnation plane, the profile becomes more and more uniform, and already at $z = -3$ mm from the stagnation plane, the profile shows an 8 mm-wide region centered on the centerline where $U = 1.57 \pm 0.25$ m/s, and flow uniformity is assured. The radial profiles of the axial (u') and radial (v') velocity rms, are also reported in Fig. 2 (right). The axial velocity rms increases dramatically as the stagnation plane is approached, while the radial velocity rms remains roughly constant. This implies that the flow becomes more and more non-isotropic near the stagnation plane, which is a stagnation flow property that cannot be influenced. The uniformity also decreases, but a, 8-mm wide region can still be considered uniform, implying that a portion of the flame will be subject to uniform mean and fluctuating strain rates. Criticisms raised on the turbulent counterflow configuration include the fact that the level of turbulence that can be achieved experimentally is modest and

Table 1
Characteristic parameters of a non-premixed flame.

Q_2 (SLPM)	U (m/s)	u'/U	L (m)	λ (m)	Re_L	Re_λ
90	13.7	0.23	4.3E-03	0.64E-03	882	132

that the turbulence is “young” [24,25] and exhibits peculiar time-scale ratios. Fig. 3 shows the velocity power spectrum as measured at the centerline of the bottom nozzle, at $z \sim -9$ mm (0.5 mm above the exit section), by hot-wire anemometry. It is apparent that the turbulence generation scheme succeeded in generating a range of length scales, without any peculiarities associated with the system compactness and the potential drawback of “young turbulence”. The estimated integral scale, L , is about 4.0 mm, in good agreement with previous measurements [21], while the Taylor length scale, λ , is about 0.6 mm. The corresponding turbulent Reynolds numbers are, respectively, $Re_L \sim 900$ and $Re_\lambda \sim 130$, which are almost one order of magnitude larger than in the published literature in opposed jet burners. These characteristic parameters and the volumetric flow rate are listed in Table 1.

In the light of these results, it is clear that the design improvements discussed in Section 3 are sufficient to ensure that a healthy level of turbulence, along with a good degree of uniformity, can be sustained in these environments. As a result, there is no reason why the counterflow scenario should not contribute to shed light on the turbulent combustion conundrum and provide a complementary scenario to the more common jet flames that have been the subject of the majority of studies to date.

4.2. Non-premixed and partially premixed flame phenomenology

Fig. 4 shows the flame phenomenology under different conditions: quasi-laminar, with no turbulence generator in either stream (top left); with the turbulence generator in only the top stream (top middle and right); and with the turbulence generator in both streams (bottom pictures). The seeded olive oil drops for the PIV measurements disappear at 570 K, leaving a dark region straddling the flame. In the absence of turbulence generators, the flame does not show any wrinkling. In the case of a single turbulent generator, the turbulent structures interact with the flame, inducing some wrinkling, with distinct vortex-like structures being also visible

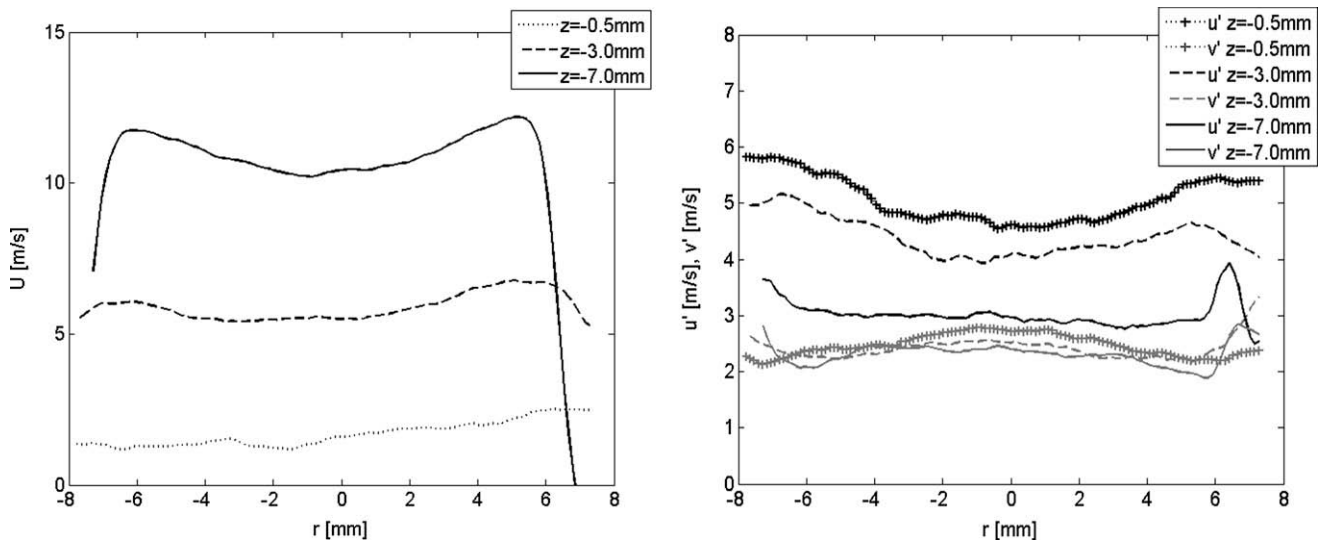


Fig. 2. Mean axial velocity (left), axial and radial velocity rms (right) vs. radial position, at different distances from the stagnation plane mean position, taken as $z = 0$. Plain line: 0.5 mm from the stagnation plane; dashed line: 3 mm from the stagnation plane; plus symbol: 7 mm from the stagnation plane. Darker lines in the figure on the right indicate axial velocity rms component. Measurements performed under cold conditions.

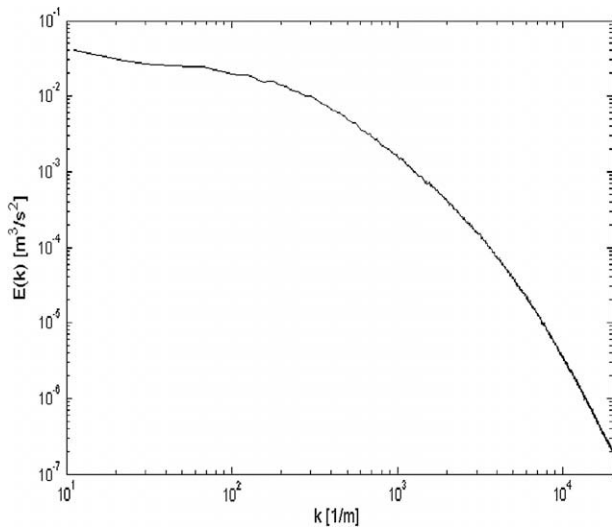


Fig. 3. Velocity power spectrum in wavenumber space, as measured 0.5 mm above the bottom nozzle exit section.

(top row, rightmost picture). With turbulence generators on both sides, intense flame wrinkling is shown with both turbulent fields interacting and separate burning “islands” are also visible (bottom row, rightmost picture).

Fig. 5 shows another interesting phenomenon that can be systematically studied in these flames, by weakening them with increased inert dilution and increasing the inert mole fraction in the fuel stream to 0.75: highly fluctuating strain rates induce local extinction in the flame, as indicated by the interruptions in the droplet-free, dark area that is no longer simply connected. These extinction events remains local under these experimental conditions, as they do not cause global extinction and are symptomatic of conditions of partial premixing, since the unburned reactants have an opportunity to premix locally, possibly yielding the estab-

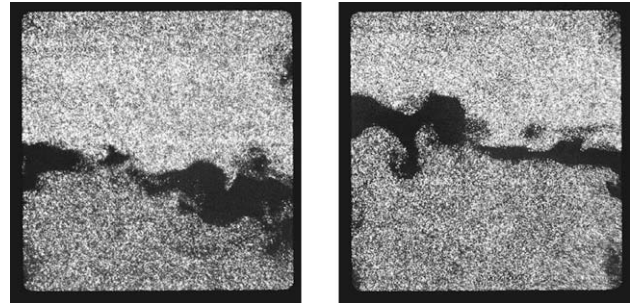


Fig. 5. PIV raw images of oil droplets showing evidence of local extinction/reignition, with droplets penetrating the dark high-temperature region.

lishment of turbulent edge flames when the extinction hole heals itself.

The lack of tracers in the flame did not allow for the measurement of the velocity field from these images. Therefore another dataset was acquired under the same conditions, switching oil droplets with alumina particles. It is well known that PIV with solid particles in a combustion environment suffers from high spurious vector yield, as a consequence of the strong drop in particle number density within the flame. The need of filtering out the spurious vector and replacing them with interpolated ones, causes the vector field to be less accurate. It should be noted, that the strong seed density difference can also be exploited to locate local extinction events, which will appear here as higher density regions in the reactive zone, characterize by low particle density. The radial profiles of the axial mean velocity, at $z = -7, -3, -1$ mm from the mean position of the stagnation plane (**Fig. 6**, left) again show that the flow becomes more and more uniform as it approaches the flame, in agreement with the cold flow measurements, indicating that the flame, at least within several mm from the centerline, is indeed subject to reasonably homogeneous mean flow conditions. The slight lack of symmetry, more evident in the $z = -0.5$ mm profile, is a consequence of a minor misalignment between the top and bottom nozzles. The present asymmetry does not alter the flow

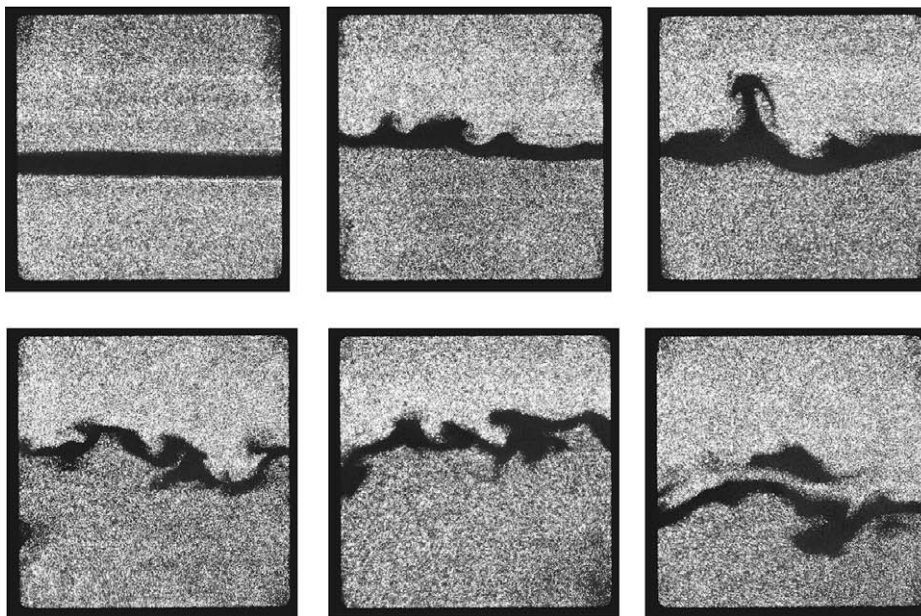


Fig. 4. PIV raw images showing different phenomenology for different combinations of turbulence generation plates (see text for details): quasi-laminar, with no turbulence generator in either stream (top left); with the turbulence generator in only the top stream (top middle and right); and with the turbulence generator in both streams (bottom pictures).

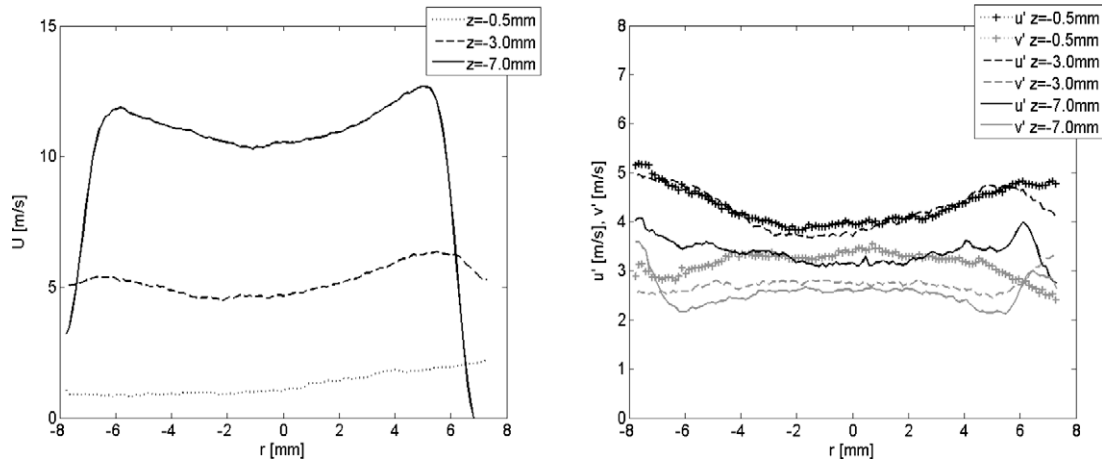


Fig. 6. Mean axial velocity (left), axial and radial velocity rms (right) vs. radial position, at different distances from the stagnation plane mean position, taken as $z = 0$. Plain line: 0.5 mm from the stagnation plane; dashed line: 3 mm from the stagnation plane; +: 7 mm from the stagnation plane. Darker lines in the figure on the right indicate axial velocity rms component. Measurements performed under burning conditions.

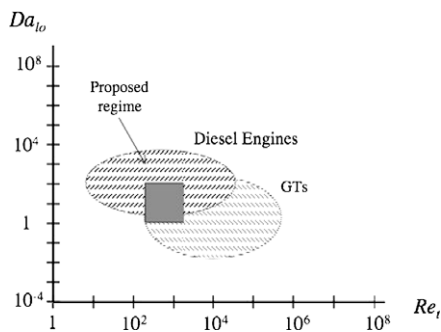


Fig. 7. Achievable regime in the Williams-Klimov diagram.

structure and has no impact on our results, nevertheless to allow for proper numerical modeling, the system is being improved by mounting the nozzles on separates translational stages, which will allow for careful alignment.

The radial profiles of axial velocity rms (Fig. 6, right) are in good agreement with the cold flow profiles (Fig. 2, right), up to $z = -3$ mm, while the $z = -0.5$ mm profile shows a strong attenuation, which is probably a consequence of both the heavier filtering/interpolation operations and possibly flame-induced turbulence attenuation.

Our initial goal was to push the envelope into a regime overlapping that of practical applications. We can now explore conditions that we were able to achieve, based on the characteristic quantities that were estimated in Table 1. As mentioned earlier, the demonstrated turbulent Reynolds numbers are about one order of magnitude larger than typical values in the literature in similar experiments to date. Under local extinction conditions, the Damköhler number based on the integral scale, $Da = (L/u')/(D/S_L^2)$, where u' is a characteristic turbulent fluctuation velocity, L is the integral scale, and D/S_L^2 is a characteristic chemical time based on a mean diffusivity and the laminar flame speed, must be of unity order. For more stable flames, this non-dimensional number will be much larger. As a result, the experiments covered the domain highlighted by the square in Fig. 7, overlapping conditions of relevance to practical systems, such as Diesel engines and gas turbines (ovals in the same figure) [37].

In summary, by introducing a properly designed and carefully positioned turbulence generator in each counterflowing stream, high turbulence intensities are achieved, without compromising the uniformity of conditions near the flame centerline. By using

pure oxygen on the oxidizer side, flames can be stabilized at high velocities of the impinging streams. The combination of these two factors leads to highly turbulent flames with well-defined and well-characterized conditions. For typical values of the feed stream composition and bulk strain under which a turbulent flame can be stabilized, at a stoichiometric mixture fraction of 0.67, 0.56 and 0.51, with pure oxygen on the oxidizer side and CH_4/N_2 on the fuel side, the bulk extinction strain rate were 460, 791 and 1600 s^{-1} , respectively, below which stable burning in either non-premixed or partially premixed mode could be achieved.

4.3. Premixed flames

When the two counterflowing jets consist of identical premixed reactant mixtures, two turbulent twin flames are stabilized on each side of the stagnation plane. As for their laminar counterparts, distinct ignition and extinction limits exist for such flames. These limits are primarily set by the strain rate that, in turn, is controlled by the nozzle separation, d , and the mean inlet velocity, U . These two variables, normalized by the inner inlet diameter, d_i , and by the flame speed, S_L , respectively, are plotted in Fig. 8. Although no turbulence variable explicitly appears in Fig. 8, since the turbulent intensity $u'/U \approx 0.23$ for all conditions, the role of the turbulent

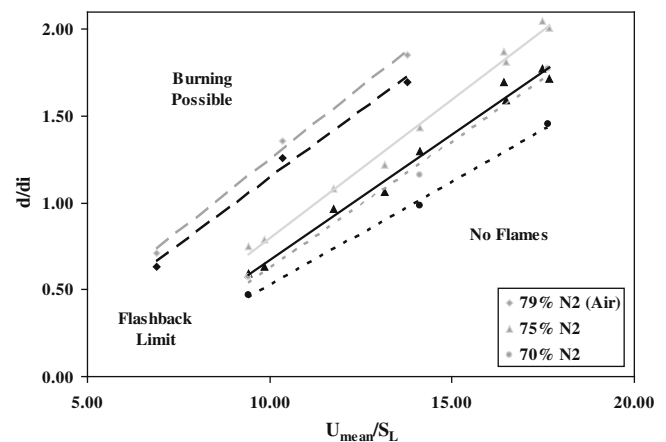


Fig. 8. Ignition (black) and extinction (grey) limits of counterflow premixed flames for various mixture dilutions: 79% N_2 (air) (diamonds), 75% N_2 (triangles) and 70% N_2 (dots).

fluctuations is implicitly taken into account by the abscissa that can be reinterpreted as u'/S_L once it is multiplied by this constant factor. For a given set of conditions, that is for fixed values of d , U and equivalence ratio, ignition was attempted with an external pilot flame. If ignition was successful, the flame was turned off, the nozzles were moved by a 1/4-mm step closer to each other, and the process was repeated till the limit strain rate was reached, beyond which no ignition was possible. Similarly, under burning conditions, for a given set of conditions, the nozzles were moved closer to each other by a 1/4-mm step. If burning conditions were preserved, the burners were brought one step closer and the process was repeated till the extinction point was reached. That point was defined when the turbulent flame would extinguish within 30 s after the nozzle displacement, that is, after a period 6 orders of magnitude larger than the integral timescale. Too short (large) a value of d/d_i (U/S_L or u'/S_L) results in an excessive bulk strain rate that may either prevent ignition or cause extinction. As a result the region to the right of the interpolating lines corresponds to strain rates that are too large for flames to stabilize. Vice versa, relatively low strain rate conditions to the left of the lines interpolating the data correspond to burning conditions. The two regions are separated by (extinction/ignition) limit lines parametrized in terms of the inert mole fraction in the “air” of the feed streams. The dataset for each level of dilution pertain to flames spanning a range of val-

ues of the equivalence ratio. Contrary to the laminar twin flames, whose ignition is possible at lower strain rates than extinction, the ignition limits of the turbulent twin flames are reached at larger bulk strain rates than those of the extinction limits. In the region between the ignition and extinction limits there exists a regime where the turbulent twin flames can be ignited but would rapidly extinguish shortly thereafter. As the inert concentration is decreased and combustion is inherently more robust, the extinction/ignition limit curves shift to the right toward conditions of larger mean flows and corresponding larger strain. Generally, these limits are related to how changes in composition affect the robustness of the flame and its structure. They depend on the mixture composition in a complex manner that cannot be rationalized only in terms of thermal effects. The issue is being addressed computationally in ongoing work in our laboratory and will be the subjects of a companion article.

The phenomenology of the premixed turbulent counterflow flames is particularly influenced by the turbulent Reynolds number Re_t and by the bulk strain rate K_{bulk} as illustrated in Fig. 9 showing a series of OH two-dimensional images, with the radical spatial distributions at various conditions of turbulent Reynolds number and bulk strain rates. From a to e, images are shown at progressively larger turbulent Reynolds numbers and bulk strain rates. Fig. 9a–d shows a stoichiometric flame in “air” with a nitrogen mo-

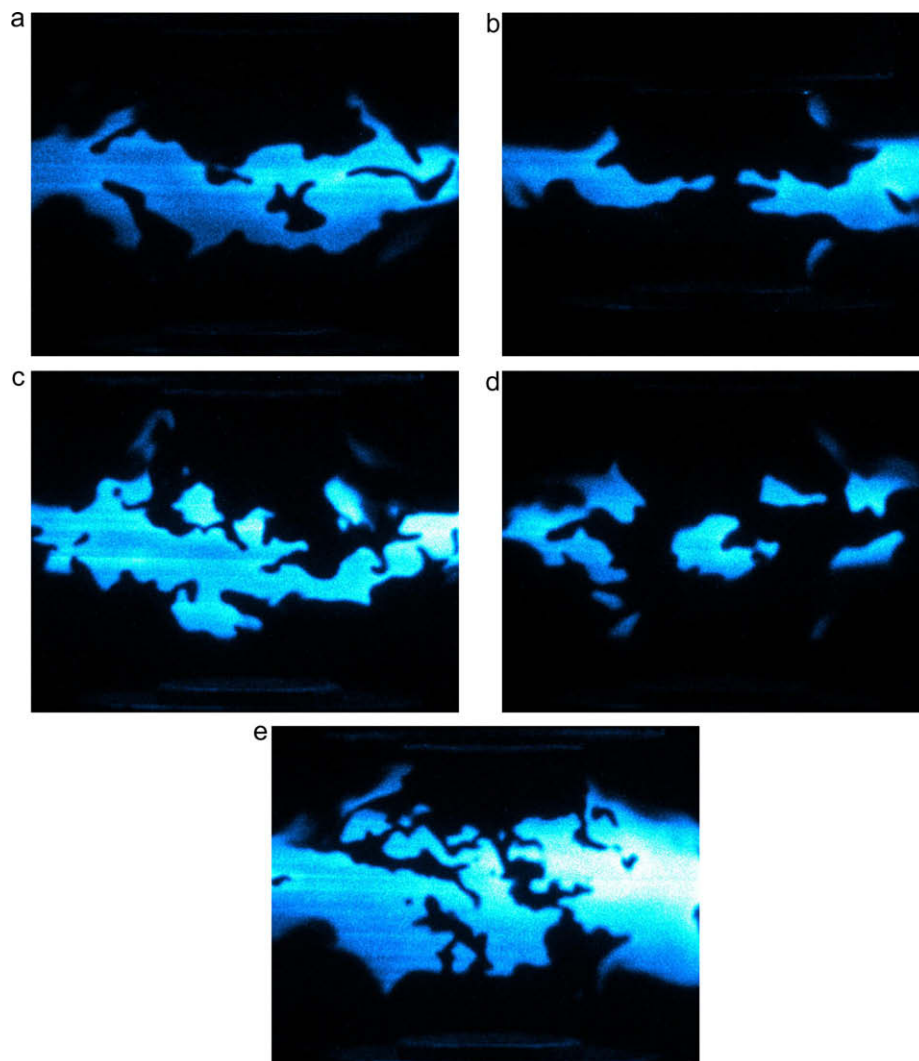


Fig. 9. Two-dimensional images of OH in counterflow premixed flames: (a) $Re_t = 350$, $K_{\text{bulk}} = 420/\text{s}$, (b) $Re_t = 350$, $K_{\text{bulk}} = 630/\text{s}$, (c and d) $Re_t = 660$, $K_{\text{bulk}} = 630/\text{s}$, (e) $Re_t = 1050$, $K_{\text{bulk}} = 900/\text{s}$.

lar fraction of 0.75. At a low turbulent Reynolds number $Re_t = 350$, flame wrinkling is less pronounced (Fig. 9a and b). Since the magnitude of the turbulent fluctuations u' is greater than the laminar flame speed S_L with $u'/S_L > 4$, the largest turbulent eddies are able to roll up the flame front locally. Occasionally, two parts of the flame are transported against each other, forced to connect and yield a pocket of fresh reactants. At a low bulk strain rate of 450 s^{-1} corresponding to a distance between the nozzles of 25 mm, the separation between the two turbulent flames is sufficiently large for the entire fresh reactant pocket to be contained in the space occupied by the hot products (Fig. 9a). Decreasing the nozzles separation to 16.5 mm, which results in a bulk strain rate $a = 630 \text{ s}^{-1}$, forces the two turbulent flames closer to each other. The space occupied by the products of combustion becomes too narrow to encompass any pocket of fresh reactants. Instead, the two turbulent flames connect locally and, as a result, fresh reactants leak across the stagnation plane (Fig. 9b). Subsequently, the reactants are either carried away by the mean flow field or the “holes” in the flames heal themselves. The situation is deceptively similar to the one of local extinction of turbulent non-premixed flames reported in Fig. 5, but it is fundamentally different since the premixed flames are *not* locally extinguished by the turbulent eddies. In fact, the flame front is generally characterized by steep gradients of the fluorescence intensity. If the flame front were extinguished, hot products and fresh reactants would be mixing locally, which should result in a diffuse OH LIF signal. On the contrary, the same steep gradients of the OH LIF signal of an unextinguished flame are observed around the holes (cf. Fig. 10).

The twin flames fall within the flamelet regimes of turbulent premixed combustion [6]. The turbulent Karlovitz number $Ka_t = (u'/S_L)^{3/2} \cdot (l_f/L)^{1/2}$, where L is the integral length scale and l_f is the laminar flame thickness, is limited to small values of order unity. Ultimately, further increases in the bulk strain rate result in the complete extinction of the turbulent twin flames. At larger Reynolds numbers, the flames are characterized by more intense corrugation and smaller radii of curvature because smaller eddies become capable of wrinkling the flame fronts (Fig. 9c). The frequency/density of local reactant leakage across the stagnation plane also increased and combustion tends to take place in distributed regions (Fig. 9d). Access to significantly larger Reynolds number regimes on the order of a thousand is possible if the turbulent Karlovitz number remains of order unity, which can be achieved by changing the equivalence ratio and the mixture dilution in order to increase the laminar flame speed proportionally to the gain in turbulence fluctuations. Fig. 9e shows a snapshot of a turbulent flame operated at an equivalence ratio of 0.8, with “air” with an N_2 mole fraction of 0.70, and at $Re_t = 1050$. As compared to the low Reynolds number case in Fig. 9a, the flame appears significantly more “shredded”.

The merging of the flames at large strain rates and the inability to explore a wide range of Karlovitz numbers prompted us to modify the burner and replace the bottom half of it with a ceramic burner through which the exhaust gases of a premixed flame that was stabilized upstream passed. In that way, single turbulent counterflow flames could be systematically investigated in a configuration in which a fresh mixture was flown against combustion products. A comprehensive examination of the behavior of such flames as a function of Re_t and Ka_t , as well as of the heat loss on the burnt side whose temperature and composition on the burnt side both of which can be independently controlled, is currently under way and will be reported in a subsequent article.

5. Compactness of the combustion domain

One of the critical advantages of the proposed configuration is the compactness of the domain in which combustion takes place.



Fig. 10. Long-exposure photograph of C_2H_4 non-premixed flames at comparable cold $Re_t \sim 10^3$ and $Re_0 \sim 10^4$ in counterflow (left) and co-flow (right) configurations. Both photographs are reproduced in the same scale.

To prove this point, it is useful to compare the counterflow configuration with the far more common jet flame that is abundantly documented in the literature. To make the comparison fair, one has to scale the two systems appropriately from a turbulence standpoint, namely by ensuring comparable Re_t . For the purpose of this discussion, we will make scaling considerations for cold, and less ambiguous, conditions. The velocity along the centerline decays as $U(x) = 5.8U_j/(x - x_0)/d$, where $x - x_0$ is a distance from the jet virtual origin at x_0 and the jet half-width, $\delta/2$, grows proportionally to x as $\delta/2(x) = 0.094(x - x_0)$ [38]. A characteristic turbulent integral scale is $0.7\delta/2$ in the longitudinal direction and $0.3\delta/2$ in the transverse direction. We will use the first for Reynolds number estimates. If one considers that the turbulent velocity fluctuations is typically at 25% of the local mean flow, we can now construct a turbulent Reynolds number as

$$\begin{aligned} (Re_t)_{\text{Co-flow}} &= \frac{0.7 \cdot \delta/2(x) \cdot 0.25U(x)}{\nu} = 0.175 \cdot Re_{\delta/2} \\ &= 0.096 \frac{U_j d}{\nu} = 0.096 \cdot Re_0, \end{aligned} \quad (4)$$

in which its dependence with respect to the engineering Reynolds, Re_0 , based on the burner diameter has been made explicit. This turbulent Reynolds number is constant throughout the flow field, that is, it is independent of x , the longitudinal coordinate, which is a peculiarity of the scaling of turbulent jets under cold conditions.

Fig. 10 shows a comparison between long-exposure photographs of two C_2H_4 non-premixed flames, one in counterflow, the other as a piloted jet flame. Table 2 reports critical parameters for these flames: the total volumetric flow rate of the fuel, \dot{Q}_F , the fuel mole fraction, X_F , the engineering Reynolds number, Re_0 and the turbulent Reynolds number, Re_t . Both pictures are reproduced in the same scale to evidence the dramatic difference, by a factor of roughly 50, in the cylindrical volume of the chemiluminescent regions at comparable Re_t in the two configurations. As mentioned earlier, this feature is useful with respect to the diagnostic implementation since the experimentalist does not have to scan large volumes with a measurement probe, nor make tessellations of multiple two-dimensional images to cover the entire flow field with an acceptable resolution. The anticipated advantage, however, is dramatic from a computational viewpoint. The factor of 50 in difference between computational volumes translates in computational cost savings of *multiple orders of magnitude*, based on the number of nodes that are necessary for a resolved computation. But the advantage is even more substantial in two respects. First, the need for a piloted flame in the co-flow configuration poses notorious problems computationally that are difficult to solve because one needs to pose realistic boundary conditions near the burner surface. The problem is completely circumvented in counterflow since the stabilization is aerodynamic, so long as adiabaticity is preserved. As the photograph in Fig. 10 shows, that is the case since the turbulent brush does not touch the boundaries. Furthermore, the spacing between the two burners can be extended to twice the burner diameter without affecting the flame stability. Therefore, the preservation of adiabaticity is assured. Second, the boundary conditions can be better controlled in counterflow, by adopting (cooled) flanges, for example, so that the temperature can be accurately specified and structured grids can be employed in the computational work. So long as the system remains adiabatic, simple boundary conditions need to be specified, except for the details of the velocity field including turbulent fluctuations. In the co-flow case, on the other hand, to account properly for entrainment effects, the computational domain will have to be extended significantly also in the radial direction, with yet additional computational cost.

Under burning conditions, the situation is more complex: in the jet flame $U(x)$ decays at a slower rate, which results in lower entrainment rate, and, most importantly, the kinematic viscosity increases as a result of the heat release rate and the temperature increase. As a result, $Re_{s/2}$ is no longer constant and generally decreases by as much as one order of magnitude with respect to cold conditions, prompting in some cases a re-laminarization of the flow field [39]. The lowering of Re_t as the flame is approached applies also to the counterflow configuration. Since the thickness of the mixing layer scales with $\delta \sim (D/\chi)^{1/2}$, where D is a suitably defined turbulent diffusivity and χ is the scalar dissipation rate, and since χ is typically much larger in the counterflow configuration because of the large strain rates throughout the flow field (see Table 1), this relaminarization effect may be confined to a smaller region of the combustion domain, unlike the co-flow counterpart.

Table 2

Some characteristic figures for the comparison of the counterflow and co-flow non-premixed flames.

Configuration	\dot{Q}_F (SLPM)	X_F	Re_0	Re_t
Counterflow	8.5	0.1	9480	1050
Co-flow	5.3	0.15	10,400	995

6. Implications for real fuels

Presently, we can broadly classify combustion research into two categories: complex, and inevitably turbulent, fluid mechanics, but simple chemical kinetics (invariably, H_2 or CH_4 oxidation) [4,5,7]; or, the reverse, simple, and inevitably laminar, fluid mechanics, but complex kinetics, including real fuels such as blends of large hydrocarbons and aromatics [40–42]. The turbulent counterflow flame has the necessary pre-requisites to bridge the gap between these two “camps”, and is uniquely suited to start facing the greater challenge of *complex fluid mechanics and complex chemical kinetics*, to become a benchmark for testing and validating computational codes, including DNS, in the not too distant future. The computational advantages were evidenced in the previous section. Clearly, for a given computational cost (inclusive of time and memory requirements) the turbulent counterflow flame will permit the inclusion of increasingly more complex kinetics and perhaps the consideration of real fuels, albeit with simplified kinetics.

With the prospect for a more diversified source of fossil fuels in the future, beyond oil and natural gas, it is clear that the burning of a broad range of fuels will pose new challenges to the implementation of their combustion, which will necessitate fundamental studies in well-defined and well-controlled environments. The proposed counterflow system may become particularly useful also in this respect. Real fuels such as kerosenes and jet fuel, on which considerable research is being focused, contain large amounts of aromatics that are notoriously prolific in soot production. Adding soot to turbulence would compound modeling challenges. In addition, laser diagnostics would be also adversely affected by the presence of soot and even of broadly fluorescent soot precursors, such as PAHs, that would complicate the implementation of laser-induced fluorescence of commonly imaged combustion intermediates such as OH and CH [43]. As a result, there is a dual, experimental and computational, need to keep soot formation at bay.

In this context, there is one additional advantage that is intrinsic of the counterflow configuration: soot suppression. There are multiple means to achieve this goal in the counterflow configuration. By operating at high strain rates, on the order of 1000 s^{-1} , which is inevitable for healthy turbulence, the average residence time is lowered to one millisecond or less, which is inherently advantageous to suppress the relatively slow soot chemistry. The non-premixed flames that were discussed in Section 4 typically required oxygen-enriched oxidizers, if not pure oxygen, for them to be stabilized under conditions of large strain rate. To keep the temperature within reasonable limits, one has to dilute the system by switching the bulk of the inert from the oxidizer side to the fuel stream. This feed stream composition of diluted fuel and pure oxygen or oxygen-enriched oxidizer yields large values of the stoichiometric mixture fraction, z_f , defined as

$$z_f = \frac{1}{1 + s \frac{Y_{FF}}{Y_{OO}}}, \quad (5)$$

where s is the stoichiometric mass ratio of oxygen to fuel, Y_{FF} and Y_{OO} are the feed stream mass fractions of fuel and oxygen, respectively. Large values of z_f help inhibiting soot since the flame stabilizes on the fuel side of the stagnation plane and soot particles are oxidized as they travel towards the gas stagnation plane and eventually outside of the combustion domain [44]. The ability to study the flame structure of jet fuel in the absence of soot, despite the fuel significant aromatic content, was demonstrated in counterflow laminar flames [40,41]. The approach should work also in the turbulent counterpart because of the more favorable conditions from the perspective of soot suppression of large strain rates and short residence times.

Conversely, in the co-flow system, mean residence times are much longer. Although operation at large z_f is feasible also in this configuration, its implementation is far more problematic than in counterflow. For example, burning in pure oxygen or in an oxygen-rich atmosphere will pose experimental and safety challenges in the control of a co-flow stream of relatively large diameters for the reasons discussed in Section 5, which will result in operation at exceedingly large flow rates.

7. Conclusions

The feasibility of establishing highly turbulent flames in a counter-current configuration has been demonstrated. Conditions can cover the whole gamut from non-premixed flames to premixed ones. High blockage plates, if properly designed and positioned, can be used to generate high turbulent Reynolds numbers, preserving flow uniformity. Stable flames at bulk strain rates on the order of thousands of s^{-1} can be stabilized by using oxygen-enriched mixtures. Local extinction holes are triggered by highly fluctuating local strain rate under both non-premixed and premixed feed streams. The configuration shows a rich phenomenology, which makes it a very useful target for model testing. Scaling considerations suggest that turbulent Reynolds number conditions of practical systems such as IC engines and gas turbines can be established in a compact, bench-top experiment amenable to computational modeling and even direct numerical simulation, with dramatic gains by comparison with traditional jet flames. Low residence times, as a result of the large strain rates, and large oxygen concentration in the oxidizer stream allow for soot-free flames even under non-premixed conditions, which bodes well for the exploration of combustion of real and soot-prone fuels.

Acknowledgments

The authors gratefully acknowledge: the financial support of ACS/PRF (Grant #FA9550-06-1-0018) and of DARPA/ARO (Grant #DAAD19-01-1-0664, Dr. Richard J. Paur, Program Manager); technical discussions with Dr. Kailas Purushothaman; and the help of Mr. N. Bernardo in the construction of part of the hardware.

References

- [1] Available from: <<http://www.ca.sandia.gov/TNF>>.
- [2] Available from: <<http://eetd.lbl.gov/aet/combustion/workshop/workshop.html>>.
- [3] R.W. Bilger, Turbulent diffusion flames, *Ann. Rev. Fluid Mech.* 21 (1989) 101–135.
- [4] R.W. Bilger, Future progress in turbulent combustion research, *Prog. Energy Combust. Sci.* 26 (2000) 367–380.
- [5] R.W. Bilger, S.B. Pope, K.N.C. Bray, J.F. Driscoll, Paradigms in turbulent combustion research, *Proc. Combust. Inst.* (2004) 30.
- [6] N. Peters, *Turbulent Combustion*, Cambridge University Press, Cambridge (MA), 2000.
- [7] P. Libby, F.A. Williams, *Turbulent Reacting Flows*, Academic Press, London, 1994.
- [8] J. Vinckier, A. Van Tiggelen, Structure and burning velocity of turbulent premixed flames, *Combust. Flame* 12 (1968) 561–568.
- [9] P.J. Goix, L. Talbot, Turbulent counterflow diffusion flame structure and dilution effects, *Combust. Sci. Technol.* 79 (1991) 175–194.
- [10] E. Mastorakos, A.M.K.P. Taylor, J.H. Whitelaw, Extinction and temperature characteristics of turbulent counterflow diffusion flames with partial premixing, *Combust. Flame* 91 (1992) 40–52.
- [11] E. Mastorakos, A.M.K.P. Taylor, J.H. Whitelaw, Scalar dissipation rate at the extinction of turbulent counterflow nonpremixed flames, *Combust. Flame* 91 (1992) 55–64.
- [12] E. Mastorakos, A.M.K.P. Taylor, J.H. Whitelaw, Extinction of turbulent counterflow flames with reactants diluted by hot products, *Combust. Flame* 102 (1995) 101–114.
- [13] L.W. Kostiuk, K.N.C. Bray, T.C. Chew, Premixed turbulent combustion in counterflowing streams, *Combust. Sci. Technol.* 64 (1989) 233–241.
- [14] L.W. Kostiuk, K.N.C. Bray, R.K. Cheng, Experimental study of premixed turbulent combustion in opposed streams, Part I – Nonreacting flow field, *The Combustion Institute*, 1993, pp. 377–395.
- [15] L.W. Kostiuk, K.N.C. Bray, R.K. Cheng, Experimental study of premixed turbulent combustion in opposed streams, Part II – Reacting flow field and extinction, *Combust. Flame* 91 (1993) 396–409.
- [16] E. Korusoy, J.H. Whitelaw, Extinction and relight in opposed flames, *Exp. Fluids* 33 (2002) 75–89.
- [17] J. Erkstejn, J.Y. Chen, C.P. Chou, J. Janicka, Modeling of turbulent mixing in opposed jet configuration: one-dimensional Monte Carlo probability density function simulation, *Proc. Combust. Inst.* 28 (2000) 141–148.
- [18] F.A. Maury, P.A. Libby, Nonpremixed flames in stagnating turbulence, part I – the $k-\epsilon$ theory with equilibrium chemistry for the methane–air system, *Combust. Flame* 102 (1995) 341–345.
- [19] A. Kempf, H. Forkel, J.Y. Chen, A. Sadiq, J. Janicka, Large-eddy simulation of a counterflow configuration with and without combustion, *Proc. Combust. Inst.* 28 (2000) 35–40.
- [20] D. Geyer, A. Dreizler, J. Janicka, A.D. Permana, J.Y. Chen, *Proc. Combust. Inst.* 30 (2005) 711–718.
- [21] D. Geyer, A. Kempf, A. Dreizler, J. Janicka, *Proc. Combust. Inst.* 30 (2005) 681–689.
- [22] D. Geyer, A. Kempf, A. Dreizler, et al., Turbulent opposed-jet flames: a critical benchmark experiment for combustion LES, *Combust. Flame* 143 (2005) 524–548.
- [23] K.N.C. Bray, M. Champion, P.A. Libby, Flames in stagnating turbulence, in: P. Libby, F.A. Williams (Eds.), *Turbulent Reacting Flows*, Academic Press, London, 1994.
- [24] K.N.C. Bray, M. Champion, P.A. Libby, Premixed flames in stagnating turbulence, part II. The mean velocities and pressure and Damköhler number, *Combust. Flame* 112 (1998) 635–654.
- [25] K.N.C. Bray, M. Champion, P.A. Libby, Premixed flames in stagnating turbulence, part IV: a new theory for the Reynolds stresses and Reynolds fluxes applied to impinging flows, *Combust. Flame* 120 (2000) 1–18.
- [26] K. Sardi, A.M.K.P. Taylor, J.H. Whitelaw, Conditional scalar dissipation statistics in a turbulent counterflow, *J. Fluid Mech.* 361 (1998) 1–24.
- [27] A.N. Lipatnikov, J. Chomiak, Are premixed turbulent stagnation flames equivalent to fully developed ones? a computational study, *Combust. Sci. Technol.* 174 (2002) 3–26.
- [28] S. Menon, N. Patel, Subgrid modeling for simulation of spray combustion in large-scale combustors, *AIAA J.* 44 (2006) 709–723.
- [29] B.D. Videto, D.A. Santavicca, A turbulent flow system for studying turbulent combustion processes, *Combust. Sci. Technol.* 76 (1991) 159–641.
- [30] C.K. Law, *Combustion Physics*, Cambridge University Press, Cambridge (MA), 2006.
- [31] A.V. Oppenheim, R.W. Schafer, *Discrete-Time Signal Processing*, Prentice-Hall, Upper Saddle River, NJ, 1989.
- [32] M.J. Barrett, D.K. Hollingsworth, On the calculation of length scales for turbulent heat transfer correlation, *J. Heat Transfer – Trans. ASME* 123 (2001) 878–883.
- [33] L.H. Benedict, R.D. Gould, Towards better uncertainty estimates for turbulence statistics, *Exp. Fluids* 22 (1996) 129–136.
- [34] F. Jorgensen, How to measure turbulence with hot-wire anemometers, *A Practical Guide*, Dantec Dynamics, 2002.
- [35] H.H. Bruun, *Hot-wire Anemometry: Principles and Signal Analysis*, Oxford University Press, London, 2000, pp. 127–130.
- [36] R.P. Lindstedt, D.S. Luff, J.H. Whitelaw, Flow Turbul. Combust. 74 (2005) 169–194.
- [37] F.A. Williams, Some recent studies in turbulent combustion, in: A. Yoshida (Ed.), *Smart Control of Turbulent Combustion*, Springer, Tokyo, 2000, pp. 1–12.
- [38] S.B. Pope, *Turbulent Flows*, Cambridge University Press, Cambridge (MA), 2000.
- [39] L. Muniz, M.G. Mungal, Effects of heat release and buoyancy on flow structure and entrainment in turbulent nonpremixed flames, *Combust. Flame* 126 (2001) 1402–1420.
- [40] J.A. Cooke, M. Bellucci, M.D. Smooke, A. Gomez, A. Violi, T. Faravelli, E. Ranzi, *Proc. Combust. Inst.* 30 (2005) 439–446.
- [41] H. Bufferand, L. Tosatto, B.L. Mantia, M.D. Smooke, A. Gomez, Experimental and computational study of methane counterflow diffusion flames perturbed by trace amounts of jet fuel and jet fuel surrogates under nonsooting conditions, *Combust. Flame*, in press, doi:10.1016/j.combustflame.2009.03.006.
- [42] S. Jahangirian, C.S. McEnally, A. Gomez, Experimental study of ethylene counterflow diffusion flames perturbed by trace amounts of jet fuel and jet fuel surrogates under incipiently sooting conditions, *Combust. Flame*, in press, doi:10.1016/j.combustflame.2009.03.003.
- [43] D. Han, M.G. Mungal, Simultaneous measurements of velocity and CH distributions. Part 1: jet flames in co-flow, *Combust. Flame* 132 (2003) 565–590.
- [44] B.M. Kumfer, S.A. Skeen, R.L. Axelbaum, *Combust. Flame* 154 (2008) 546–556.